



1 **Multi-Satellite Retrieval of SSA using OMI-MODIS algorithm**

2 Kruthika Eswaran^{1,2*}, Sreedharan Krishnakumari Satheesh^{1,2} and Jayaraman Srinivasan^{1,2}

3 ¹ Centre for Atmospheric and Oceanic Sciences, Indian Institute of Science, Bangalore, India

4 ² Divecha Centre for Climate Change, Indian Institute of Science, Bangalore, India

5 *Correspondence to: Kruthika Eswaran (kruthika.eswaran89@gmail.com)

6 **Abstract** - Single scattering albedo (SSA) represents a unique identification of aerosol type and
7 aerosol radiative forcing. However, SSA retrievals are highly uncertain due cloud contamination
8 and aerosol composition. Recent improvement in the SSA retrieval algorithm has combined the
9 superior cloud masking technique of Moderate Resolution Imaging Spectroradiometer (MODIS)
10 and the better sensitivity of Ozone Monitoring Instrument (OMI) to aerosol absorption. The
11 combined OMI-MODIS algorithm has been validated over a small spatial and temporal scale
12 only. The present study validates the algorithm over global oceans for the period 2008-2012. The
13 geographical heterogeneity in the aerosol type and concentration over the Atlantic Ocean, the
14 Arabian Sea and the Bay of Bengal was useful to delineate the effect of aerosol type on the
15 retrieval algorithm. We also noted that OMI overestimates SSA when absorbing aerosols were
16 present closer to the surface. We attribute this overestimation to data discontinuity in the aerosol
17 height climatology derived from Cloud-Aerosol Lidar and Infrared Pathfinder Satellite
18 Observations (CALIPSO) satellite. OMI uses pre-defined aerosol heights over regions where
19 CALIPSO climatology is not present leading to overestimation of SSA. The importance of
20 aerosol height was also studied using the Santa Barbara DISORT radiative transfer (SBDART)
21 model. The results from the joint retrieval were validated with ground-based measurements and
22 it was seen that OMI-MODIS SSA retrievals were better constrained than OMI only retrieval.



23 1. Introduction

24 Aerosols of different types are spatially distributed heterogeneously and at different altitudes in
25 the atmosphere. Depending upon their properties, certain aerosols (biomass and carbon) warm
26 the atmosphere by absorbing radiation, while other aerosols (sea salts and sulphates) cool the
27 atmosphere by scattering radiation (Ramanathan et al., 2001). Due to the opposing effects on the
28 atmosphere aerosols can have either net warming or cooling effect on the global climate
29 depending upon the aerosol type, concentration and vertical distribution. Effect of aerosols on the
30 global climate is measured by 'aerosol radiative forcing' (the perturbation to the earth's radiation
31 budget caused by the presence of aerosols). Positive forcing implies atmospheric warming and
32 vice-versa. (Liao and Seinfeld, 1998; Podgorny and Ramanathan, 2001; Satheesh, 2002; Johnson
33 et al., 2003; Kim et al., 2004; Moorthy et al., 2004; Meloni et al., 2005; Satheesh and Moorthy,
34 2005; Seinfeld and Pandis, 2006; Satheesh et al., 2008; Chand et al., 2009; Mishra et al., 2015).
35 According to the climate assessment report, the estimation of aerosol radiative forcing is a major
36 cause of uncertainty in the estimation of climate sensitivity and therefore presents a great
37 impediment to climate modeling (IPCC, 2013). The uncertainty is largely due to the lack of
38 accurate measurement of the scattering and absorbing properties of the aerosols (Cooke and
39 Wilson, 1996; Menon et al., 2002; Chung and Seinfeld, 2002; Bond and Sun, 2005).

40 The Single Scattering Albedo (SSA), (the fraction of radiation scattered out of total
41 extinction of radiation) is used to distinguish the scattering and absorbing properties of aerosols.
42 SSA represents a unique fingerprint of the type of aerosol and its radiative forcing (Hansen et al.,
43 1997; Haywood et al., 1997; Myhre et al., 1998). In general, purely scattering aerosols have SSA
44 value of approximately 1 while highly absorbing aerosols have SSA less than 0.7. However,
45 SSA values lack high certainty (Bond and Bergstrom, 2006; Bond et al., 2013). Uncertainties in



46 SSA measurements are due to factors such as cloud contamination, instrumentation error and
47 aerosol modification due to atmospheric processes. Better SSA retrievals (both in-situ and
48 satellite-based) are required to reduce the uncertainty in SSA for a more accurate estimation of
49 aerosol forcing; particularly over regions influenced by a variety of air masses. There is also a
50 need for accurate spectral aerosol absorption measurements, which is required to validate SSA
51 derived from satellite measurements (Bergstrom et al., 2007).

52 Studies on the various direct measurements of SSA and their uncertainty evaluation have
53 been performed previously (Horvath, 1993, Heintzenberg et al., 1997; Moosmuller et al., 2009).
54 Along with ground-based retrievals of SSA, there have been other indirect methods to retrieve
55 the parameter using satellite images and observations (Table 1).

56 Though these previous studies on ground-based measurements have brought a fundamental
57 understanding to the estimation of amounts of aerosols / aerosol chemistry, their restricted spatial
58 and temporal extent is a major limitation. Moreover, these studies also have a reduced
59 availability of scenes for indirect retrievals. Some techniques are limited due to cloud
60 contamination while others operate only under specific conditions (e.g. presence of sun glint).
61 This presents a need for better SSA retrieval algorithms that overcome the present technical
62 limitations and that can be applied on a global scale. The global extent of observations from
63 satellites has increased the spatial extent of the observations (Kaufman et al., 2002a). Though the
64 satellite-based retrievals have been shown to be extremely successful over the majority of ocean
65 and land regions, they still have a limited success over deserts and ice sheets. Over deserts and
66 ice-sheets, high surface reflectance affects the satellite retrievals in visible spectrum. To counter
67 this, SSA is retrieved in UV spectrum (330 nm to 400 nm) over these regions (Torres et al., 1998,
68 2007). In UV spectrum, the upwelling radiances are highly sensitive to the aerosol absorption



69 and also have a lower influence of surface albedo (Torres et al., 2007). SSA retrieval in UV
70 spectrum also avoids difficulties encountered in scenarios where there are large surface
71 reflectance contrasts.

72 The quality of OMI SSA retrievals is affected by sub-pixel cloud contamination and the
73 spectral surface albedo (Torres et al., 2007). To counter the problems and uncertainties in the
74 OMI SSA retrieval (Table 2), Satheesh et al. 2009 used retrieval from multiple satellites. They
75 used combined retrieval from OMI-MODIS since sensors on each of the satellites have their own
76 strengths and both fly within few minutes of each other in the A-train constellation (Stephens et
77 al., 2002). The better cloud-screened retrieval of AOD from MODIS (Levy et al., 2003) and the
78 high sensitivity of OMI to aerosol absorption were used to develop a hybrid algorithm to retrieve
79 SSA (Satheesh et al., 2009). The study was performed over Atlantic Ocean and Arabian Sea for
80 the year 2006. A comparison of the retrieved aerosol height with aircraft measurements showed
81 that OMI-MODIS was more accurate than OMI. Gasso and Torres (2016) performed a detailed
82 analysis of the OMI UV product retrievals over oceans and island sites. They compared the OMI
83 retrieved AOD with MODIS and AERONET AODs. This work used the OMI-MODIS algorithm
84 for only two particular cases over and near Africa to understand how the assumption of aerosol
85 height and shape affected AOD and SSA retrievals. It was found that when the actual height from
86 satellite Lidar was used instead of climatological values and when the shape of dust aerosols was
87 assumed to be non-spherical, the retrievals by OMI agreed better with other observations
88 including OMI-MODIS method. While the OMI-MODIS algorithm has been used in calculating
89 aerosol radiative forcing (Satheesh et al., 2010) over oceanic regions surrounding India and used
90 in retrieving SSA over land (Narasimhan and Satheesh, 2013) as well as used to understand the
91 retrievals of OMI UV products for two particular cases (Gasso and Torres, 2016), a detailed



92 analysis of the algorithm on a larger spatial and temporal scale has not been done so far.

93 The current work applies the OMI-MODIS algorithm to retrieve SSA on a global scale. It is
94 applied over global oceans from 2008-2012. Regional analysis over the Atlantic, the Arabian Sea
95 and the Bay of Bengal has been done by incorporating the aerosol layer height and the type of
96 aerosols. A simulation study using Santa Barbara DISORT Radiative Transfer (SBDART) model
97 was performed to highlight the importance of aerosol layer height. After estimating SSA values
98 using the OMI-MODIS algorithm, the present study then uses cruise measurements of SSA from
99 the Integrated Campaign for Aerosols, Gases and Radiation Budget (ICARB) and winter ICARB
100 campaigns over Arabian Sea and Bay of Bengal in 2006 and 2009 to validate the same (Moorthy
101 et al., 2008, 2010).

102 **2. Data**

103 **2.1. OMI**

104 The Ozone Monitoring Instrument (OMI) on board the Aura satellite was launched in 2004. For
105 OMI measurements two aerosol inversion schemes are used- OMI near UV (OMAERUV)
106 algorithm and the multi-wavelength (OMAERO) algorithm (Torres et al., 2007). The OMAERO
107 algorithm uses 19 wavelengths in the range of 330-500 nm to retrieve corresponding aerosol
108 characteristics. For the present study we have used the OMAERUV algorithm which uses
109 measurements at two wavelengths 354 nm and 388 nm. The reason behind choosing these
110 wavelengths is the high sensitivity of upwelling radiances to aerosol absorption and the lower
111 influence of surface in measurements due to low reflectance values in the UV region. This gives
112 a unique advantage of retrieving aerosol properties over ocean and land including arid and semi-
113 arid regions (Torres et al., 1998; 2007).

114 The products derived from the algorithm include AOD, absorption aerosol optical depth



115 (AAOD) and single scattering albedo (SSA). These are derived from pre-computed reflectance
116 values for different aerosol models. Three major types of aerosols have been used - Desert dust,
117 carbonaceous aerosols from biomass burning and sulphate-based aerosols. Each type has seven
118 models of SSA. The retrieved products of OMAERUV are sensitive to the aerosol layer height
119 (Torres et al., 1998). The values are derived at surface and at 1.5, 3.0, 6.0 and 10.0 km above the
120 surface. The best estimate of the values of AOD, AAOD and SSA of a particular choice of
121 aerosol vertical distribution are evaluated.

122 Due to the high sensitivity of SSA retrieval to the assumption of aerosol height and aerosol
123 type, the OMI algorithm was improved (Collection 003-PGE V1.4.2, Torres et al., 2013) using
124 climatology of aerosol layer height from CALIPSO (Cloud-Aerosol Lidar and Infrared
125 Pathfinder Satellite Observations) along with carbon monoxide (CO) measurements from AIRS
126 (Atmospheric Infrared Sounder) for better identification of carbonaceous aerosols. Torres et al.
127 (2013) showed that the combined use of AIRS CO measurements and OMI Aerosol Index (AI)
128 retrievals, helped in identifying the type of absorbing aerosol. Thus smoke layers were identified
129 when values of AI and CO measurements were high and during events of high AI and low CO
130 values, the aerosols were identified as dust. The AIRS CO measurements were also used to
131 identify large aerosol loading which was otherwise represented as clouds by the OMAERUV
132 algorithm. Using collocated observations of OMI and CALIOP, Torres et al. (2013) estimated the
133 height of elevated absorbing aerosols for a 30-month period from July 2006 to December 2008.
134 An effective aerosol height was calculated from the attenuated backscatter weighted with
135 average height using the CALIOP 1064 nm measurements. The 30-month climatology of aerosol
136 height was used in the OMAERUV algorithm and validated with Aerosol Robotics Network
137 (AERONET) observations (Torres et al., 2013). The results showed that there was improvement



138 in the retrievals. The original aerosol height assumptions were used in the algorithm over regions
139 where the climatology was unavailable. For the present study we have used the improved
140 OMAERUV algorithm along with AOD, SSA retrievals at different aerosol heights and as well
141 as the best estimates of AOD and SSA.

142 **2.2. MODIS**

143 The Moderate Resolution Imaging Spectrometer (MODIS) instrument in Aqua satellite was
144 launched in 2002. This instrument, with 36 spectral channels has a unique ability to retrieve
145 aerosol properties with better accuracy over both land and ocean (Remer et al., 2005; Levy et al.,
146 2003). Of these, seven channels (0.47-2.13 μm) are used to retrieve aerosol properties over ocean
147 (Tanre et al., 1997).

148 As described in Remer et al., (2005), before the retrieval algorithm, masking of sediments,
149 clouds and ocean glint is performed to separate valid pixels from bad ones. The retrieval
150 algorithm of MODIS (also called the inversion procedure) has been described in detail
151 previously (Tanre et al., 1997; Levy et al., 2003; Remer et al., 2005). The algorithm uses a 'look-
152 up table' (LUT) approach, i.e., for a set of aerosol and surface parameters, radiative transfer
153 calculations are performed. Spectral reflectance derived from the LUT is compared with
154 MODIS-measured spectral reflectance to find the 'best' (least-squares) fit. The resulting
155 combination of modes provides the aerosol model from which size distribution, properties
156 including spectral optical depth, effective radius etc. is derived. The product used from MODIS
157 is the Level 2 aerosol (MYD04, Collection 5.1) product. The parameter chosen is
158 'Effective_Optical_Depth_Average_Ocean' which provides the aerosol optical depth over ocean
159 at seven wavelengths. The value is the average of all the solutions in the inversion procedure
160 with the least-square error < 3%.



161 A combination of OMI and MODIS helps indirectly in counteracting the cloud
162 contamination problem and also uses the strength of the individual sensors – OMI's sensitivity to
163 aerosol absorption combined with the better cloud screening of MODIS and accurate retrieval of
164 AOD, and aerosol size (Satheesh et al., 2009; Narasimhan and Satheesh, 2013).

165 3. Algorithm

166 MODIS has high spatial pixel resolution of 10km x 10km at nadir (and a cloud mask at 500m
167 and 1km resolution) whereas OMI has a resolution of 13 km x 24 km. This results in a pixel
168 being prone to cloud contamination which overestimates AOD and underestimates single
169 scattering co-albedo (1-SSA) (Torres et al., 1998). However, AAOD can be retrieved in the
170 presence of small cloud contamination since there is cancellation of errors (Torres et al., 2007).

171 The higher accuracy in MODIS retrieval over ocean is due to the fact that it has large
172 number of channels in the Shortwave Infrared (SWIR) region (Tanre et al., 1997; Remer et al.,
173 2005; Levy et al., 2003). While OMI is highly sensitive to aerosol absorption in the near-UV
174 region, the accuracy in the retrieval of AAOD depends on the aerosol layer height assumption.
175 OMI provides AOD and AAOD at different heights as prescribed by various aerosol types
176 (Torres et al., 2007).

177 The assumption of aerosol layer height in the OMI algorithm restricts the retrieval of AOD
178 and AAOD. Using this as basis, the approach proposed in Satheesh et al. (2009) used MODIS
179 AOD as an input to the OMI retrieval algorithm, so that the inversion, now checked, can use the
180 information to infer the aerosol layer height and SSA. To know the SSA at 388 nm, the AOD
181 used should also be at the same wavelength. Satheesh et al. (2009) extrapolated MODIS AOD
182 and compared the estimated UV AOD with high quality ground-based AERONET observations.
183 The deviation between MODIS-extrapolated AOD and AERONET AOD was greater at higher



184 AERONET AOD values. This was attributed to the presence of large number of fine-mode
185 aerosols which affected AOD at UV wavelengths. Hence to improve the linear extrapolation,
186 information on the aerosol spectral curvature was also included. This was achieved by using an
187 average regression equation to correct the MODIS AOD (Satheesh et al., 2009; Equation 3).
188 They showed that MODIS AOD can be linearly extrapolated to 388 nm and use the corrected
189 AOD as input to the OMI retrieval algorithm. The present work uses the same algorithm as
190 proposed by Satheesh et al. (2009) to retrieve SSA over the oceans for the region 60S-60N and
191 180W-180E from December 2007-November 2012. The methodology is described in detail in the
192 following section.

193 **4. Methodology**

194 The AOD for ocean obtained from the Level 2 aerosol product of MODIS (MYD04) was used.
195 Using linear extrapolation, AOD at 388 nm (hereafter, AOD₃₈₈) was calculated from AOD at
196 seven wavelengths ranging from 0.47-2.13 μm , after the inclusion of aerosol spectral curvature
197 defined in Satheesh et al. (2009). OMI provides AOD and SSA for five different aerosol layer
198 heights starting from surface and at 1.5, 3.0, 6.0 and 10.0km (AOD_{omi} and SSA₃₈₈). It also
199 provides the best estimate of SSA calculated for a particular aerosol vertical distribution
200 (SSA_{omi}).

201 For the present study, polar regions are not included and hence pixels from both OMI and
202 MODIS that are outside the 60S-60N and 180W-180E region are excluded. Pixels with invalid or
203 missing values are also excluded. To reduce computation time the various parameters extracted
204 from the data were re-gridded onto a uniform grid of $0.5^\circ \times 0.5^\circ$ within the region of study. For
205 both the satellites, this procedure was repeated for each swath data which were then combined to
206 calculate the daily means.



207 The daily data from collocated MODIS and OMI were utilised in the final algorithm. As
208 mentioned before OMI provides AOD and SSA for five different aerosol layer heights. Using
209 AOD_{388} as the reference, the corresponding aerosol layer height was calculated from the five
210 AOD_{omi} values through linear interpolation. This height is then used as a reference to find the
211 SSA using interpolation from the set of SSA_{388} values. Finally, this SSA ($SSA_{omi-modis}$), and the
212 best estimate of SSA (SSA_{omi}) were compared to each other.

213 5. Results

214 The spatial distribution of SSA retrieved using OMI is shown in Fig. 1a. The values are averaged
215 over five years and plotted seasonally.

216 The SSA retrieved using OMI-MODIS algorithm is shown in Fig. 1b.

217 SSA over open oceans is close to 1 due to the presence of large amount of sea-salt and
218 sulphate. Closer to land, a variety of aerosols are present which results in SSA varying from 0.75
219 to ~1. Over the oceans, separating ocean colour effects and aerosol concentrations is difficult.
220 Hence the OMI algorithm retrieves only if there are enough absorbing aerosols present, i.e. AI
221 ≥ 0.8 (Torres et al., 2013). Only pixels whose quality has been assigned as 0 or the highest
222 quality by OMI have been used. Since 2007, observations have been affected by a phenomenon
223 called the *row anomaly* which reduces the quality of radiance at all wavelengths. The points
224 flagged for row anomaly are not used in this study. Further information about row anomaly can
225 be found in Jethva et al. (2014). Thus, the retrievals did not cover the entire globe. From Fig. 1a it
226 can be seen that majority of the valid SSA retrievals were over major aerosol sources in the
227 world and not over remote oceanic regions like central equatorial Pacific or Antarctic ocean. The
228 major sources include the vast biomass outflow over Atlantic Ocean from the west coast of
229 Africa, the dust over Arabian Sea from the arid areas of Arabia & Africa and the dust blown over



230 Atlantic Ocean from Sahara. Other regions like the east coast of China, Bay of Bengal are
231 influenced by a variety of anthropogenic aerosols during different seasons. Both the algorithms
232 capture the major oceanic regions which are influenced by large number of aerosols.

233 Two important regions over oceans influenced by a variety of aerosols are the Atlantic
234 Ocean and the oceans around the Indian subcontinent. The new approach was used over these
235 regions- Atlantic (5N-30N; 60W-20W) (ATL) and Arabian Sea and Bay of Bengal (0-25N; 55E-
236 100E) (ARBOB).

237 **5.1. Difference in SSA retrieval algorithms during different seasons**

238 To understand how the OMI-MODIS algorithm compared with the retrieval using existing OMI
239 algorithm, the difference between $SSA_{\text{omi-modis}}$ and SSA_{omi} (ΔSSA) averaged over five years for
240 different seasons is shown in Fig. 2.

241 During March-April May (MAM) and June-July-August (JJA), there is a longitudinal
242 gradient in ΔSSA from the coast of Sahara towards the open Atlantic Ocean. Kaufman et al.
243 (2002a) showed that closer to the coast of Africa, aerosols are more absorbing than those away
244 from the coast. The difference in the type of aerosols as we move away from the coast could be
245 one of the reasons for the gradient in ΔSSA . The ΔSSA changes sign with season. This was
246 attributed to the dominating presence of either natural aerosols (JJA) or anthropogenic aerosols
247 (DJF).

248 Both ATL and ARBOB regions are influenced by the type of aerosols which result in a
249 complex mixture and eventually resulting in the variation in SSA distribution over each season.
250 While the spatial plot of ΔSSA in Fig. 2 represents the regions where maximum and minimum
251 differences are located around the globe, a distribution plot provides the ranges of ΔSSA which
252 dominate and which do not. The distribution of ΔSSA for different seasons averaged over five



253 years (2008-2012) is plotted in Fig. 3a and 3b for the regions- ATL and ARBOB respectively.

254 DJF shows a strong positive bias in both the regions, JJA shows a negative bias and the
255 other two seasons show negligible bias. While dust outflows dominate over ATL, over ARBOB –
256 Arabian Sea is affected by dust at higher altitudes and sea-salt near the surface whereas the Bay
257 of Bengal is influenced mainly by continental and marine aerosols. The change in the sign of
258 difference could either be due to the difference in type of aerosol or the assumption in aerosol
259 layer height (ALH). To understand what type of aerosols affect these water bodies, trajectory
260 analysis is done. This helps in identifying major sources of aerosols during each season.

261 **5.2. Trajectory analysis**

262 **5.2.1. Atlantic (ATL)**

263 The region in the tropical Atlantic is surrounded by the Sahara Desert in the east and the
264 North America in the west. The transport of dust from Sahara over Atlantic Ocean is a regular
265 occurrence (Prospero and Carlson, 1972). Aerosol distribution over Atlantic is also affected by
266 the African Easterly Waves and other atmospheric dynamics in Africa (Zuluaga, 2012). The
267 Atlantic region is influenced by not only dust from Sahara, but also by aerosols from biomass
268 burning off the coast of Africa and aerosols from industries and pollution from America. Thus,
269 there is a complex mixture of aerosols over the Atlantic Ocean during any season. A 7-day back
270 trajectory analysis was performed at a location in the box (15N; 45W) using the online Hybrid
271 Single-Particle Lagrangian Integrated Trajectory (HYSPLIT) model for the years 2009-2010.
272 The trajectory was computed for different seasons at 3 heights – 500m, 1500m and 2500m above
273 mean sea level (MSL). The Atlantic Ocean was divided into four quadrants representing the
274 regions of possible sources of aerosols 1) North America, 2) Central/South America, 3) North
275 Africa and 4) Southern Africa (Fig. 4). The influence of these aerosol sources over Atlantic



276 Ocean is estimated as the percentage of trajectories that start from each region respectively. The
277 maximum influence is given in bold (Table 2).

278 From Table 2 it can be seen that the major source of aerosols over the Atlantic Ocean is the
279 dust outflow from the Sahara Desert (Prospero, 1996). Extreme heating over Sahara creates a
280 layer of instability (Saharan Air Layer) which lifts the dust particles enabling long-range
281 transport. Far off the coast the warm dust layer encounters a cooler, wetter air layer causing
282 inversion. This results in the dust layer being intact over Atlantic Ocean (Prospero and Carlson,
283 1972). Field experiments like the trans-Atlantic Aerosol and Ocean Science Expeditions
284 (AEROSE I and II) showed the outflow of dust during spring and summer along with other trace
285 gases and biomass aerosols (Morris et al., 2006). However, dust is not the only aerosol present in
286 the region of study. Using an airborne differential absorption LIDAR (DIAL) system, Harriss et
287 al. (1984), found that there is advection of anthropogenic pollutants from North America to the
288 North Atlantic Ocean. Advanced very high-resolution radiometer (AVHRR) instrument on the
289 National Oceanic and Atmospheric Administration (NOAA) 11 satellite provides global aerosol
290 information. From that data it was found that large plumes over Atlantic Ocean were attributed to
291 the pollution from North America and Europe. During spring and summer, the large outflow was
292 due to the dust outbreak from Sahara and Sahel. Biomass burning from southern Africa, South
293 America and anthropogenic emissions from North and Central America dominated the aerosol
294 loading over Atlantic Ocean during winter (Husar et al., 1997). The MODIS instrument onboard
295 the Terra satellite was first used to study the transport and deposition over Atlantic Ocean. It was
296 found that during winter, the dust which was present was mixed with the biomass aerosols from
297 Sahel and closer to the coast of North America the dust was influenced by the pollution and
298 smoke from the continent. Pure dust was present over the ocean during summer months



299 (Kaufman et al., 2005). From Table 2 it is also seen that the dust dominated at all heights except
300 during winter when the pollution from North America dominated at higher altitudes.

301 **5.2.2. Arabian Sea and Bay of Bengal (ARBOB)**

302 The Arabian Sea and the Bay of Bengal are oceanic regions on the west and east coast of
303 India respectively. Both regions are influenced by various types of aerosols during different
304 seasons. The Arabian Sea has been dominated by dust aerosols and is influenced by high levels
305 of dust during certain seasons as seen from satellite images (Sirocko and Sarnthein, 1989). Pease
306 et al. (1998) studied the geochemistry and the transport of various dust samples during different
307 cruises in different seasons. During winter and summer, the pattern of aerosol transport was
308 similar to that of the Indian monsoon pattern – northeasterly (winter) and southwesterly
309 (summer). Thus, the major sources of aerosols were the Arabian Peninsula (including Saharan
310 dust and Middle East) and Indian sub-continent in summer and winter respectively. The mean 7-
311 day back trajectory using HYSPLIT model from a point over Arabian Sea (15N; 65E) was
312 performed for each season of 2010 and at three different heights (500m, 1500m and 2500m
313 above MSL). Only one year is performed since the trajectory analysis over Atlantic Ocean
314 showed that the aerosol pathways did not vary much between years. The Arabian Sea region was
315 divided into four quadrants – 1) Arabian Peninsula and North Africa, 2) Southern Africa, 3)
316 Indian sub-continent and 4) Indian Ocean and Southeast Asia (Fig. 5). Similar to Table 2,
317 influence of different aerosol source regions over the Arabian Sea is given in Table 3.

318 Similar to Pease et al. (1998), Tindale and Pease (1999) found that transport of aerosols near
319 the surface followed the surface wind currents. The dust content was low near the surface during
320 summer due to the presence of Föhn jet, but the general dust concentrations were higher than
321 other oceanic regions. During winter, the winds are predominantly north and north easterly and



322 hence results in transport of aerosols from India/Pakistan/Afghanistan onto Arabian Sea.
323 However, the presence of anticyclonic circulation over Arabia (20N; 60E) results in north
324 westerly winds transporting dust over Arabian Sea (Rajeev et al., 2000). The spring time (March-
325 April-May) is the transition between northeast and southwest monsoon. The winds become south
326 westerlies which result in the advection of aerosols from open Indian Ocean or near Somalia. At
327 higher altitudes (above the Findlater jet) dust transport occurs from Arabia. During summer, the
328 southwest monsoon wind patterns carry aerosols all the way from southeast/east Indian Ocean
329 (mainly sea-salt). As the altitude increases, the wind patterns change a little due to aerosols
330 coming from southwest Indian Ocean/Somalia. Above the Findlater jet, as explained by Tindale
331 and Pease (1999), dust transport occurs from Arabian Peninsula (Table 3).

332 Being an integral part in the Indian Summer Monsoon, studies over Bay of Bengal is
333 important especially the role of aerosols in the local climate change. While Arabian Sea is
334 dominated by dust and oceanic aerosols and only anthropogenic aerosols during SON, studies
335 have shown that Bay of Bengal is influenced by various air masses associated with Asian
336 monsoon system (Krishnamurti et al., 1998). The synoptic meteorological conditions over Bay of
337 Bengal have been studied in detail by Moorthy et al. (2003) and Satheesh et al. (2006). Similar to
338 the other two regions, mean 7-day back trajectory analysis from a point over (15N; 90N) was
339 performed for each season of 2010 and at three different heights (500m, 1500m and 2500m
340 above MSL). The four quadrants representing the various aerosol source regions are 1)
341 India/Arabian Peninsula, 2) Indian Ocean, 3) North/Northeast India and East Asia and 4)
342 Southeast Asia (Fig. 6). Table 4 represents the influence of aerosol source regions over Bay of
343 Bengal.

344 The north westerly winds occur from west to east in the Indo-Gangetic Plain (IGP) and due



345 to subsidence, the aerosols are trapped in the east during winter (Dey and Di Girolamo, 2010; Di
346 Girolamo et al., 2004). The IGP with its heavy population and large number of industries acts as
347 a source for anthropogenic aerosols which are transported to Bay of Bengal during winter
348 (Kumar et al., 2013). Along with mineral dust from Arabian Peninsula, biomass aerosols from
349 Southeast Asia are also transported to the bay. Field experiments like ICARB (Moorthy et al.,
350 2008) during the spring time (pre-monsoon) showed transports of aerosols from the Arabian
351 Peninsula and also presence of elevated aerosols (anthropogenic and natural) over Bay of Bengal
352 (Satheesh et al., 2008). The post monsoon season acts as a transition from the summer to winter
353 monsoon. The winds during September are still south westerlies and during October weak
354 westerlies are present (Lawrence and Lelieveld, 2010). This results in transportation of aerosols
355 from Indian Ocean and Arabian Sea. Thus, from Table 4 it can be seen that both anthropogenic
356 aerosols (from IGP, Southeast Asia) and natural aerosols (marine and dust) are present over Bay
357 of Bengal during different seasons.

358 **5.3. Role of Aerosol Layer Height in SSA retrieval**

359 Satheesh et al. (2009) devised a new algorithm to improve the retrieval of SSA using
360 combined OMI and MODIS data. They used MODIS-predicted UV AOD as the input to improve
361 the original OMI algorithm, which was constrained by the assumption of aerosol layer height.
362 Over the Atlantic, the values retrieved from both algorithms showed reasonably good agreement.
363 However, over the Arabian Sea only when there was considerable loading of dust, the OMI AOD
364 and MODIS AOD had agreement suggesting that during other seasons, the assumption of aerosol
365 height could be wrong. Satheesh et al. (2009) also found that over Arabian Sea the aerosol layer
366 height (ALH) derived from OMI-MODIS algorithm agreed well with aircraft measurements
367 when compared to OMI SSA retrieval. In the current work, the aerosol layer height (ALH) was



368 calculated for OMI, using the best estimate of SSA retrieved from OMI. The difference in
369 aerosol layer height between OMI-MODIS and OMI was plotted with the difference in SSA (Fig.
370 7a and 7b). The colorbar in the figure represents height estimated using the OMI-MODIS
371 algorithm.

372 Most important observation from this analysis is that OMI overestimates SSA at lower ALH
373 (retrieved by OMI-MODIS algorithm) and underestimates SSA at higher ALH. The latest version
374 of OMI algorithm uses CALIPSO climatology of aerosol layer height for better accuracy.
375 However, over regions where this is not available, pre-defined aerosol height has been used
376 based on the type of aerosol assumed. For industrial sulphate aerosols exponential profile with
377 2km scale height is assumed with a similar profile with 1.5km scale height for oceanic aerosols.
378 For biomass type aerosols, a Gaussian distribution with peak at 3km is used. Dust aerosols are
379 assumed to have two-single Gaussian distributions with maximum at heights 3 and 5km. It has
380 been shown by Gasso and Torres (2016) that when the actual aerosol height was 1.5km more
381 than climatological or assumed height, OMI retrieved higher SSA.

382 It can be seen from Figs. 7a and 7b, the blue coloured circles represent height between
383 surface to ~ 2km. In this range it is seen that the height assumed by OMI is > 1.5km compared to
384 the one estimated by OMI-MODIS. Thus, OMI overestimates SSA compared to the OMI-
385 MODIS retrieval. This overestimation is due to the predefined vertical profiles. Thus, there are
386 errors with regard to both the aerosol layer height as well as the type of aerosol in the OMI
387 algorithm. In the OMI algorithm, the highest uncertainty in retrieving SSA is due to aerosol layer
388 height and aerosol type (Torres et al., 2002). Using ground-based LIDAR measurements,
389 Satheesh et al. (2009) concluded that OMI-MODIS retrieved height agreed better with
390 observations than OMI.



391 The importance of ALH and SSA in the calculation of TOA flux is studied using Santa
392 Barbara DISORT (SBDART) model (Ricchiazzi et al., 1998). For the same tropical environment
393 variables and surface albedo of 0.06, the SSA was varied from 0.8 to 1 and aerosol height from 0
394 to 10 km at 1 km interval. The simulations were done for a narrow band in UV (300-400nm). For
395 a constant AOD, AE (Angstrom Exponent) and asymmetry factor (0.4, 1 and 0.7 respectively),
396 TOA flux was calculated (Fig. 8). It can be seen that at any ALH, TOA flux varied with SSA in.
397 The role of ALH is important in the UV region due to the phenomena of Rayleigh scattering (van
398 de Hulst, 1981). The importance of Rayleigh scattering on the role of ALH is further shown in
399 Fig. 9. In this particular set of simulations, the Rayleigh scattering is completely removed and all
400 other parameters are kept same as in Fig. 8.

401 It can be seen that once molecular scattering is removed, the effect of ALH is also removed
402 and TOA flux depends only on SSA and other aerosol properties. This set of SBDART
403 simulations shows us how for a particular value of TOA flux, assuming different aerosol height
404 gives us different SSA values reiterating the important role of aerosol height on SSA retrievals.

405 **5.4. Validation**

406 To validate the new retrieval method of SSA using OMI and MODIS, both SSA values from
407 OMI and OMI-MODIS were compared with ground-based measurements (SSA at 450nm)
408 during Cruises in the period 2006 and 2009 in Arabian Sea and Bay of Bengal. These cruises
409 were part of the Integrated Campaign for Aerosols, gases and Radiation Budget (ICARB)
410 performed during the months of March to May 2006 and once during winter (W-ICARB) from
411 27 December 2008 to 30 January 2009 (Moorthy et al., 2008 and 2010). Since the spatial
412 coverage of OMI-MODIS and cruise measurements is less, the SSA values for both the
413 algorithms were averaged over the region of study and compared with observed SSA (Fig. 10).



414 However, the cruise measurements showed that SSA varied a lot spatially especially over Bay of
415 Bengal. Hence instead of a spatial average, the SSA values were temporally averaged for the
416 months when the cruise was performed. This was done under the assumption that during the
417 cruise period, the SSA over each location did not vary with time. For better coverage, a 1.5° box
418 was used around each location within which the mean SSA was calculated.

419 The mean SSA of OMI, OMI-MODIS and cruise measurements are calculated and the
420 difference between mean satellite SSA and mean SSA from cruise measurements are calculated
421 for OMI and OMI-MODIS algorithms separately. A statistical t-test is performed comparing the
422 respective SSA means of OMI and OMI-MODIS with SSA. The null hypothesis assumes the
423 mean SSA of OMI/OMI-MODIS is equal to the mean SSA calculated from the cruise
424 measurements. The values from Table 5 show that despite the mean difference of OMI SSA and
425 cruise SSA being ~ 0.013 , it was statistically significant at 95% significance level. On the other
426 hand the SSA retrieved using OMI-MODIS algorithm was better constrained and was closer to
427 the mean value of SSA from cruise measurements. The distribution of SSA from both the
428 satellite algorithms as well as from cruise measurements is shown in Fig. 11.

429 Using five years (2008-2012) of OMI and OMI-MODIS data for the region of Arabian Sea
430 and Bay of Bengal, SSA was retrieved and the difference between the two methods was
431 calculated and plotted against SSA from the OMI-MODIS algorithm (Fig. 12). For absorbing
432 aerosols detected by OMI-MODIS the SSA is overestimated by OMI.

433 The OMI-MODIS approach in SSA retrieval is one of the many combinations of sensors that
434 can be used in retrieving aerosol properties. A more complete approach involving better vertical
435 distribution of aerosols either from space or ground-based observations is required to reduce the
436 uncertainty further. However, with few ground-based measurements in the UV regime, validation



437 of new algorithms is still in the nascent stage.

438 **6. Summary and Conclusions**

439 Aerosol forcing depends on aerosol properties like aerosol optical depth (AOD) and single
440 scattering albedo (SSA). SSA is highly sensitive to the aerosol composition and size and as well
441 as the wavelength at which the aerosol interacts with radiation. A slight change in SSA value can
442 alter the sign of the forcing. Hence it is important to have an accurate measurement of SSA
443 globally. Ozone Monitoring Instrument (OMI) retrieves SSA in the UV spectrum. However,
444 these retrievals are affected by cloud contamination and are sensitive to aerosol layer height. To
445 resolve the issue of sub-pixel cloud contamination, Satheesh et al (2009) developed a method
446 using the combination of OMI and the Moderate Resolution Imaging Spectroradiometer
447 (MODIS) at a local scale. In the present study, we use the method developed by Satheesh et al
448 (2009) to retrieve SSA at a much larger spatial and temporal scale. The main findings from our
449 study are listed below:

- 450 1. Both OMI and OMI-MODIS algorithms retrieved SSA over regions influenced by large
451 amounts of aerosols (e.g. Atlantic Ocean – ATL; Arabian Sea and Bay of Bengal –
452 ARBOB)
- 453 2. Difference in SSA retrievals of OMI-MODIS and OMI for both regions ATL and
454 ARBOB fluctuates between positive and negative values during different seasons which
455 could be due to the difference in either the type of aerosol or aerosol height assumed. In
456 addition, a longitudinal gradient of difference in SSA retrievals is present from the coast
457 of Sahara to the open ocean during the JJA season. This could be due the difference in
458 type of aerosols near the coast and in the open ocean
- 459 3. OMI overestimates SSA at lower ALH and underestimates at higher values of ALH. Over



460 regions where CALIPSO climatology is not present, OMI uses pre-defined aerosol
461 heights based on the aerosol present. From Fig. 4 it is also seen that OMI is unable to
462 retrieve absorbing aerosols present at very low heights (< 2km) due to the already defined
463 vertical profiles.

464 4. In the UV spectrum, ALH plays a more dominant role than in the visible region due to
465 the major effect of Rayleigh scattering in UV. When Rayleigh scattering was removed,
466 ALH had no effect in both the UV and visible regions of the spectrum.

467 5. OMI-MODIS method was validated using cruise data from the ICARB and W-ICARB
468 campaigns in the Arabian Sea and Bay of Bengal. The difference between OMI SSA and
469 SSA from cruise measurements despite being small is statistically significant. OMI-
470 MODIS SSA is better constrained and is closer to the cruise measurements

471 6. It is seen that the OMI overestimates SSA when absorbing aerosols were detected by
472 OMI-MODIS and the cruise measurements.

473 Aerosol type and aerosol layer height play a very important role in the retrieval of aerosol
474 properties. Without the assumption of aerosol type or height, OMI-MODIS is able to detect
475 absorbing aerosols much better than OMI. Hence this algorithm is useful over regions dominated
476 by absorbing aerosols like Bay of Bengal during winter. The importance of aerosol height is
477 clearly demonstrated by SBDART model and the validation with ground-based measurements
478 highlighted the role of aerosol type. However, an accurate comparison and validation of such
479 retrieval algorithms can be possible only when there are more ground-based observations
480 available in the UV spectrum on a larger spatial and temporal scale.

481 **Acknowledgements**

482 The authors gratefully acknowledge the NOAA Air Resources Laboratory (ARL) for the



483 provision of the HYSPLIT transport and dispersion model used in this publication. The authors
484 are grateful to NASA data and services centre.

485 **References**

486 Bergstrom, R.W., Pilewskie, P., Russell, P.B., Redemann, J., Bond, T.C., Quinn, P.K., and Sierau,
487 B.: Spectral absorption properties of atmospheric aerosols, *Atmos. Chem. Phys.*, 7, 5937-
488 5943, 2007.

489 Bond, T.C., and Sun, H.: Can reducing black carbon emissions counteract global warming?,
490 *Environ. Sci. Technol.*, 39(16), 5921-5926, 2005.

491 Bond, T.C., and Bergstrom, R.W.: Light absorption by carbonaceous particles: An investigative
492 review, *Aerosol Sci. Tech.*, 40(1), 27-67, doi:10.1080/02786820500421521, 2006.

493 Bond, T.C., Doherty, S.J., Fahey, D.W., Forster, P.M., Bernsten, T., De Angelo, B.J., Flanner,
494 M.G., Ghan, S., Karcher, B., Koch, D., Kinne, S., Kondo, Y., Quinn, P.K., Sarofim, M.C.,
495 Schultz, M., Venkataraman, C., Zhang, H., Zhang, S., Bellouin, N., Guttikunda, S.K.,
496 Hopke, P.K., Jacobson, M.Z., Kaiser, J.W., Klimont, Z., Lohmann, U., Schwarz, J.P.,
497 Shindell, D., Storelvmo, T., Warren, S.G., and Zender, C.S.: Bounding the role of black
498 carbon in the climate system: A scientific assessment, *J. Geophys. Res.*, 118(11), 5380-
499 5552, doi:10.1002/jgrd.50171, 2013.

500 Chand, D., Wood, R., Anderson, T.L., Satheesh, S.K., and Charlson, R.J.: Satellite-derived direct
501 radiative effect of aerosols dependent on cloud cover, *Nat. Geosci.*, 2, 181–184,
502 doi:10.1038/ngeo437, 2009.

503 Chung, S.H., and Seinfeld, J.H.: Global distribution and climate forcing of carbonaceous
504 aerosols, *J. Geophys. Res.*, 107(D19), 4407, doi:10.1029/2001JD001397, 2002.

505 Cooke, W.F., and Wilson, J.J.N.: A global black carbon aerosol model, *J. Geophys. Res.*, 101,



- 506 19395-19410, doi:10.1029/96JD00671, 1996.
- 507 Dey, S., and Di Girolamo, L.: A climatology of aerosol optical and microphysical properties over
508 the Indian subcontinent from 9 years (2000–2008) of Multiangle Imaging
509 Spectroradiometer (MISR) data, *J. Geophys. Res.*, 115, D15204,
510 doi:10.1029/2009JD013395, 2010.
- 511 Di Girolamo, L., Bond, T.C., Bramer, D., Diner, D.J., Fettingner, F., Kahn, R.A., Mrtonchik, J.V.,
512 Ramana, M.V., Ramanathan, V., and Rasch, P.J.: Analysis of Multi-angle Imaging
513 SpectroRadiometer (MISR) aerosol optical depths over greater India during winter 2001-
514 2004, *Geophys. Res. Lett.*, 31(23), L23115, doi:10.1029/2004GL021273, 2004.
- 515 Diner, D.J., Beckert, J.C., Reilly, T.H., Bruegge, C.J., Conel, J.E., Kahn, R.A., Martonchik, J.V.,
516 Ackerman, T.P., Davies, R., Gerstl, S.A.W., Gordon, H.R., Muller, J.-P., Myneni, R.B.,
517 Sellers, P.J., Pinty, B., and Verstraete, M.M.: Multi-angle Imaging SpectroRadiometer
518 (MISR) instrument description and experiment overview, *IEEE T GEOSCI REMOTE*,
519 36(4), 1072-1087, doi:10.1109/36.700992, 1998.
- 520 Dubovik, O., and King, M.D.: A flexible inversion algorithm for retrieval of aerosol optical
521 properties from Sun and sky radiance measurements, *J. Geophys. Res.*, 105(D16), 20673-
522 20696, doi:10.1029/2000JD900282, 2000.
- 523 Dubovik, O., Holben, B.N., Eck, F.T., Smirnov, A., Kaufman, Y.J., King, M.D., Tanre, D., and
524 Slutsker, I.: Variability of absorption and optical properties of key aerosol types observed
525 in worldwide locations, *J. Atmos. Sci.*, 59(3), 590-608, doi:10.1175/1520-
526 0469(2002)059<0590:VOAAOP>2.0.CO;2, 2002.
- 527 Eck, T.F., Holben, B.N., Slutsker, I., and Setzer, A.: Measurements of irradiance attenuation and
528 estimation of aerosol single scattering albedo for biomass burning aerosols in Amazonia, *J.*



- 529 Geophys. Res., 103(D24), 31865-31878, doi:10.1029/98JD00399, 1998.
- 530 Gasso, S., and Torres, O.: The role of cloud contamination, aerosol layer height and aerosol
531 model in the assessment of the OMI near-UV retrievals over the ocean, Atmos. Meas.
532 Tech., 9, 3031-3052, doi:10.5194/amt-9-3031-2016, 2016.
- 533 Hansen, J., Sato, M., and Ruedy, R.: Radiative forcing and climate response, J. Geophys. Res.-
534 Atmos., 102(D6), 6831-6864, doi:10.1029/96JD03436, 1997.
- 535 Harriss, R.C., Browell, E.V., Sebacher, D.I., Gregory, G.L., Hinton, R.R., Beck, S.M., McDougal,
536 D.S., and Shipley, S.T.: Atmospheric transport of pollutants from North America to the
537 North Atlantic Ocean, Nature, 308, 722-724, doi:10.1038/308722a0, 1984.
- 538 Haywood, J.M., Roberts, D.L., Slingo, A., Edwards, J.M., and Shine, K.P.: General circulation
539 model calculations of the direct radiative forcing by anthropogenic sulphate and fossil-fuel
540 soot aerosol, J. Clim., 10, 1562-1577, doi:10.1175/1520-
541 0442(1997)010<1562:GCMCOT>2.0.CO;2, 1997.
- 542 Heintzenberg, J., Charlson, R.J., Clarke, A. D., Liousse, C., Ramaswamy, V., Shine, K.P.,
543 Wendish, M., and Helas, G.: Measurements and modelling of aerosol single-scattering
544 albedo: Progress, problems and prospects, Contrib. Atmos. Phys., 70(4), 249– 263, 1997.
- 545 Herman, B.M., Browning, R.S., and De Luisi, J.J.: Determination of the effective imaginary term
546 of the complex refractive index of atmospheric dust by remote sensing: the diffuse-direct
547 radiation method, J. Atmos. Sci., 32, 918-925, doi:10.1175/1520-
548 0469(1975)032<0918:DOEIT>2.0.CO;2, 1975.
- 549 Herman, J.R., Bhartia, P.K., Torres, O., Hsu, C., Sefstor, C., and Celarier, E.: Global distribution
550 of UV-absorbing aerosols from Nimbus 7/TOMS data, J. Geophys. Res.-Atmos., 102(D14),
551 16911-16922, doi:10.1029/96JD03680, 1997.



- 552 Horvath, H.: Atmospheric light absorption- a review, *Atmos. Environ. A-Gen.*, 27(3), 293-317,
553 doi:10.1016/0960-1686(93)90104-7, 1993.
- 554 Intergovernmental Panel on Climate Change (IPCC) (2013), *The physical science basis:
555 Contribution of Working Group I to the Fifth Assessment Report of the Intergovernmental
556 Panel on Climate Change*, In: *Climate Change (2013)*, Stocker, T.F., D. Qin, G.K. Plattner,
557 M. Tignor, S.K. Allen, J. Boschung, A. Nauels, Y. Xia, V. Bex, and P.M. Midgley (eds),
558 Cambridge University, Press: Cambridge, United Kingdom and New York, NY, USA 1535
559 pp, doi:10.1017/CBO9781107415324.
- 560 Jethva, H., Torres O., and Ahn C.: Global assessment of OMI aerosol single-scattering albedo
561 using ground-based AERONET inversion, *J. Geophys. Res.-Atmos.*, 119(14), 9020-9040,
562 doi:10.1002/2014JD021672, 2014.
- 563 Johnson, B.T., Shine, K.P., and Forster, P.M.: The semi-direct aerosol effect: Impact of absorbing
564 aerosols on marine stratocumulus, *Q. J. Roy. Meteor. Soc.*, 130, 1407-1422,
565 doi:10.1256/qj.03.61, 2003.
- 566 Kaufman, Y.J.: Satellite sensing of aerosol absorption, *J. Geophys. Res.*, 92, 4307-4317,
567 doi:10.1029/JD092iD04p04307, 1987.
- 568 Kaufman, Y.J., Tanre, D., and Boucher, O.: A satellite view of aerosols in the climate system,
569 *Nature*, 419, 215-223, doi:10.1038/nature01091, 2002a.
- 570 Kaufman, Y.J., Martins, J.V., Remer, L.A., Schoeberl, M.R., and Yamasoe, M.A.: Satellite
571 retrieval of aerosol absorption over the oceans using sunglint, *Geophys. Res. Lett.*, 29(19),
572 34-1 – 34-4, doi:10.1029/2002GL015403, 2002b.
- 573 Kaufman, Y.J., Koren, I., Remer, L.A., Tanre, D., Ginoux, P., and Fan, S.: Dust transport and
574 deposition observed from the Terra-Moderate Resolution Imaging Spectroradiometer



- 575 (MODIS) spacecraft over the Atlantic Ocean, *J. Geophys. Res.*, 110, D10S12,
576 doi:10.1029/2003JD004436, 2005.
- 577 Kim, S-W., Yoon, S-C., Jefferson, A., Won, J-G., Dutton, E.G., Ogren, J.A., and Anderson T.L.:
578 Observation of enhanced water vapour in Asian dust layer and its effect on atmospheric
579 radiative heating rates, *Geophys. Res. Lett.*, 31(18), doi:10.1029/2004GL020024, 2004.
- 580 King, M.D.: Determination of the ground albedo and the index of absorption of atmospheric
581 particulates by remote sensing. Part II: Application, *J. Atmos. Sci.*, 36, 1072-1083,
582 doi:10.1175/1520-0469(1979)036<1072:DOTGAA>2.0.CO;2, 1979.
- 583 Krishnamurti, T.N., Jha, B., Prospero J., Jayaraman, A., and Ramanathan, V.: Aerosol and
584 pollutant transport and their impact on radiative forcing over the tropical Indian Ocean
585 during the January – February 1996 pre-INDOEX cruise, *Tellus B*, 50(5): 521–542,
586 doi:10.1034/j.1600-0889.1998.00009.x, 1998.
- 587 Kumar, K.R., Sivakumar, Reddy, R.R., and Gopal, K.R.: Ship-borne measurements of columnar
588 and surface aerosol loading over the Bay of Bengal during W-ICARB campaign: role of
589 airmass transport. Latitudinal and Longitudinal Gradients, *Aerosol Air Qual Res.*, 13, 818–
590 837, doi:10.4209/aaqr.2012.08.0225, 2013.
- 591 Lawrence, M.G., and Lelieveld, J.: Atmospheric pollutant outflow from southern Asia: a review,
592 *Atmospheric Chemistry and Physics*, 10, 11017-11096, doi:10.5194/acp-10-11017-2010,
593 2010.
- 594 Levy, R.C., Remer, L.A., Tanre, D., Kaufman, Y.J., Ichoku, C., Holben, B.N., Livingston, J.M.,
595 Russell, P.B., and Maring, H.: Evaluation of the Moderate-Resolution Imaging
596 Spectroradiometer (MODIS) retrievals of dust aerosol over the ocean during PRIDE, *J.*
597 *Geophys. Res.*, 108(D19), 8594, doi:10.1029/2002JD002460, 2003.



- 598 Liao, H., and Seinfeld, J.H.: Radiative forcing by mineral dust aerosols: Sensitivity to key
599 variables, *J. Geophys. Res.-Atmos.*, 103(D24), 31637-31645, doi:10.1029/1998JD200036,
600 1998.
- 601 Meloni, D., di Sarra, A., di Lorio, T., and Fiocco, G.: Influence of the vertical profile of Saharan
602 dust on the visible direct radiative forcing, *J. Quant. Spectrosc. Ra.*, 93(4), 397-413,
603 doi:10.1016/j.jqsrt.2004.08.035, 2005.
- 604 Menon, S., Hansen, J., Nazarenko, L., and Luo, Y.: Climate effects of black carbon aerosols in
605 China and India, *Science*, 297(5590), 2250-2253, doi:10.1126/science.1075159, 2002.
- 606 Mishra, A.K., Koren, I., and Rudich, Y.: Effect of aerosol vertical distribution on aerosol-
607 radiation interaction: A theoretical prospect, *Heliyon*, e00036,
608 doi:10.1016/j.heliyon.2015.e00036, 2015.
- 609 Moorthy, K.K., Babu, S.S., and Satheesh, S.K.: Aerosol spectral optical depths over the Bay of
610 Bengal: role of transport, *Geophys. Res. Lett.*, 30(5): 1249, doi:10.1029/2002GL016520,
611 2003.
- 612 Moorthy, K.K., Babu, S.S., Sunilkumar, S.V., Gupta, P.K., and Gera, B.S.: Altitude profiles of
613 aerosol BC, derived from aircraft measurements over an inland urban location in India,
614 *Geophys. Res. Lett.*, 31(22), 10.1029/2004GL021336, 2004.
- 615 Moorthy, K.K., Satheesh, S.K., Babu, S.S., and Dutt, C.B.S.: Integrated campaign for aerosols,
616 gases and radiation budget (ICARB): an overview, *J. Earth. Syst. Sci.*, 117(1), 243-262,
617 doi:10.1007/s12040-008-0029-7, 2008.
- 618 Moorthy, K.K., Beegum, S.N., Babu, S.S., Smirnov, A., John, S.R., Kumar, K.R., Narasimhulu,
619 K., Dutt, C.B.S., and Nair, V.S.: Optical and physical characteristics of Bay of Bengal
620 aerosols during W-ICARB: spatial and vertical heterogeneities in the marine atmospheric



- 621 boundary layer and in the vertical column, *J. Geophys. Res.*, 115(D24): D24213,
622 doi:10.1029/2010JD014094, 2010.
- 623 Moosmuller, H., Chakrabarty, R.K., and Arnott, W.P.: Aerosol light absorption and its
624 measurement: A review, *J. Quant. Spectrosc. Ra.*, 110(11), 844-878,
625 doi:10.1016/j.jqsrt.2009.02.035, 2009.
- 626 Morris, V., Colon, P.C., Nalli, N.R., Joseph, E., Armstrong, R.A., Detres, Y., Goldberg, M.D.,
627 Minnett, P.J., and Lumpkin, R.: Measuring Trans-Atlantic aerosol transport from Africa,
628 *EOS Trans. AGU*, 87(50), 565-571, doi:10.1029/2006EO500001, 2006.
- 629 Myhre, G., Stordal, F., Restad, K., and Isaksen, I.S.A.: Estimation of the direct radiative forcing
630 due to sulphate and soot aerosols, *Tellus*, 50B, 463-477, 1998.
- 631 Narasimhan, D., and Satheesh, S.K.: Estimates of aerosol absorption over India using multi-
632 satellite retrieval, *Ann. Geophys.*, 31, 1773-1778, doi:10.5194/angeo-31-1773-2013, 2013.
- 633 Pease, P.P., Tchakerian, V.P., and Tindale, N.W.: Aerosols over the Arabian Sea: geochemistry
634 and source areas for Aeolian desert dust, *J. Arid Environ.*, 39(3), 477-496,
635 doi:10.1006/jare.1997.0368, 1998.
- 636 Podgorny, I.A., and Ramanathan, V.: A modeling study of the direct effect of aerosols over the
637 tropical Indian Ocean, *J. Geophys. Res.*, 106(D20): 24097-24105,
638 doi:10.1029/2001JD900214, 2001.
- 639 Prospero, J.M., and Carlson, T.N.: Vertical and areal distribution of Saharan dust over the
640 western equatorial north Atlantic Ocean, *J. Geophys. Res.*, 77(27), 5255-5265,
641 doi:10.1029/JC077i027p05255, 1972.
- 642 Prospero, J.M.: Saharan dust transport over the North Atlantic Ocean and Mediterranean: An
643 overview, In: *The Impact of Desert Dust Across the Mediterranean*, Guerzoni S., Chester



- 644 R. (Eds.), 133-151, doi:10.1007/978-94-017-3354-0_13, 1996.
- 645 Rajeev, K., Ramanathan, V., and Meywerk, J.: Regional aerosol distribution and its long-range
646 transport over the Indian Ocean, *J. Geophys. Res.-Atmos.*, 105(D2), 2029-2043,
647 doi:10.1029/1999JD900414, 2000.
- 648 Ramanathan, V., Crutzen, P.J., Kiehl, J.T., and Rosenfield, D.: Aerosols, climate and the
649 hydrological cycle, *Science*, 294(5549): 2119–2124, doi:10.1126/science.1064034, 2001.
- 650 Remer, L. A., Kaufman, Y. J., Tanre, D., Mattoo, S., Chu, D. A., Martins, J. V., Li, R. R., Ichoku,
651 C., Levy, R. C., Kleidman, R. G., Eck, T. F., Vermote, E., and Holben, B. N.: The MODIS
652 aerosol algorithm, products, and validation, *J. Atmos. Sci.*, 62, 947–973,
653 doi:10.1175/JAS3385.1, 2005.
- 654 Ricchiazzi, P., Yang, S., Gautier, C., and Sowle, D.: SBDART: a research and teaching software
655 tool for plane-parallel radiative transfer in the earth's atmosphere, *B. Am. Meteorol. Soc.*
656 79(10): 2101–2114, doi:10.1175/1520-0477(1998)079<2101: SARATS>2.0.CO;2, 1998.
- 657 Satheesh, S.K.: Aerosols and climate, *Resonance*, 7(4), 48-59, doi:10.1007/BF02836138, 2002.
- 658 Satheesh, S.K., and Moorthy, K.K.: Radiative effects of natural aerosols: a review, *Atmos.*
659 *Environ.*, 39(11): 2089–2110, doi:10.1016/j.atmosenv.2004.12.029, 2005.
- 660 Satheesh, S.K., Srinivasan, J., and Moorthy, K.K.: Spatial and temporal heterogeneity in aerosol
661 properties and radiative forcing over Bay of Bengal: Sources and role of aerosol transport,
662 *J. Geophys. Res.*, 111(D8): D08202, doi:10.1029/2005JD006374, 2006.
- 663 Satheesh, S.K., Moorthy, K.K., Babu, S.S., Vinoj, V., and Dutt, C.B.S.: Climate implications of
664 large warming by elevated aerosol over India, *Geophys. Res. Lett.*, 35(19),
665 doi:10.1029/2008GL034944, 2008.
- 666 Satheesh, S.K., Torres, O., Remer, L.A., Babu, S.S., Vinoj, V., Eck, T.F., Kleidman, R.G., and



- 667 Holben, B.N.: Improved assessment of aerosol absorption using OMI-MODIS joint
668 retrieval, *J. Geophys. Res.*, 114, D05209, doi:10.1029/2008JD011024, 2009.
- 669 Satheesh, S.K., Vinoj, V., and Moorthy, K.K.: Assessment of aerosol radiative impact over
670 oceanic regions adjacent to Indian subcontinent using multi-satellite analysis, *Adv.*
671 *Meteorol.*, 2010, Article ID 139186, pp 13., doi:10.1155/2010/139186, 2010.
- 672 Seinfeld, J.H., and Pandis, S.N.: *Atmospheric Chemistry and Physics: From air pollution to*
673 *climate change*, 2nd Ed., 1232 pp, John Wiley & Sons, Inc., Hobkoben, New Jersey, 2006.
- 674 Sirocko, F., and Sarnthein, M.: Wind-borne deposits in the northwestern Indian Ocean: Record of
675 Holocene sediments versus modern satellite data, In: *Paleoclimatology and*
676 *Paleometeorology: modern and past patterns of global atmospheric transport*, Leinen M.,
677 Sarnthein M. (Eds), 401-433, Amsterdam: Kluwer Academic Publishers, 1989.
- 678 Stephens, G.L., Vane, D.G., Boain, R.J., Mace, G.G., Sassen, K., Wang, Z., Illingworth, A.J.,
679 O'Connor, E.J., Rossow, W.B., Durden, S.L., Miller, S.D., Austin, R.T., Benedetti, A.,
680 Mitrescu, C., and CloudSat Science Team: The CloudSat mission and the A-Train: A new
681 dimension of space-based observations of clouds, precipitation, *B. Am. Meteorol. Soc.*, 83,
682 1771-1790, doi:10.1175/BAMS-83-12-1771, 2002.
- 683 Tanre, D., Kaufman, Y.J., Herman, M., and Mattoo, S.: Remote sensing of aerosol properties
684 over oceans using the MODIS/EOS spectral radiances, *J. Geophys. Res.*, 102(D14),
685 16971–16988, 1997.
- 686 Tindale, N.W., and Pease, P.P.: Aerosols over the Arabian Sea: Atmospheric transport pathways
687 and concentrations of dust and sea salt, *Deep-Sea Res. Pt. II*, 46(8-9), 1577-1595,
688 doi:10.1016/S0967-0645(99)00036-3, 1999.
- 689 Torres, O., Bhartia, P. K., Herman, J. R., and Ahmad, Z.: Derivation of aerosol properties from



- 690 satellite measurements of backscattered ultraviolet radiation. Theoretical Basis, J.
691 Geophys. Res., 103(D14), 17099–17110, 1998.
- 692 Torres, O., Decae, R., Veefkind, J.P., and de Leeuw, G.: OMI aerosol retrieval algorithm, in OMI
693 Algorithm Theoretical Basis Document: Clouds, Aerosols, and Surface UV Irradiance, 3,
694 V2, OMIATBD- 03, edited by P. Stammes, pp. 47 – 71, NASA Goddard Space Flight
695 Cent., Greenbelt, Md, 2002.
696 ([http://eosps0.gsfc.nasa.gov/eos_homepage/for_scientists/atbd/docs/OMI/ATBD-OMI-](http://eosps0.gsfc.nasa.gov/eos_homepage/for_scientists/atbd/docs/OMI/ATBD-OMI-03.pdf)
697 03.pdf)
- 698 Torres, O., Bhartia, P.K., Sinyuk, A., Welton, E.J., and Holben, B.: Total Ozone Mapping
699 Spectrometer measurements of aerosol absorption from space: Comparison to SAFARI
700 2000 ground-based observations, J. Geophys. Res., 110(D10), doi:10.1029/2004JD004611,
701 2005.
- 702 Torres, O., Tanskanen, A., Veihelmann, B., Ahn, C., Braak, R., Bhartia, P.K., Veefkind, P., and
703 Levelt, P.: Aerosols and surface UV products from Ozone Monitoring Instrument
704 observations: An overview, J. Geophys. Res., 112, D24S47, doi:10.1029/2007JD008809,
705 2007.
- 706 Torres, O., Ahn, C., and Chen, Z.: Improvements to the OMI near-UV aerosol algorithm using A-
707 train CALIOP and AIRS observations, Atmos. Meas. Tech., 6, 3257-3270,
708 doi:10.5194/amt-6-3257-2013, 2013.
- 709 Van de Hulst, H.C.: Light scattering by small particles, 496 pp., Dover publications, New York,
710 1981.
- 711 Wells, K.C., Martins, J.V., Remer, L.A., Kreidenweis, S.M., and Stephens, G.L.: Critical
712 reflectance derived from MODIS: Application for the retrieval of aerosol absorption over



713 desert regions, *J. Geophys. Res.*, 117(D3), doi:10.1029/2011JD016891, 2012.

714 Zhu, L., Martins, J.V., and Remer, L.A.: Biomass burning aerosol absorption measurements with
715 MODIS using the critical reflectance method, *J. Geophys. Res.*, 116(D7),
716 doi:10.1029/2010JD015187, 2011.

717 Zuluaga, M.D., Webster, P.J., and Hoyos, C.D.: Variability of aerosols in the tropical Atlantic
718 Ocean relative to African Easterly Waves and their relationship with atmospheric and
719 oceanic environments, *J. Geophys. Res.*, 117(D16), doi:10.1029/2011JD017181, 2012.

720

721

722

723

724

725

726

727

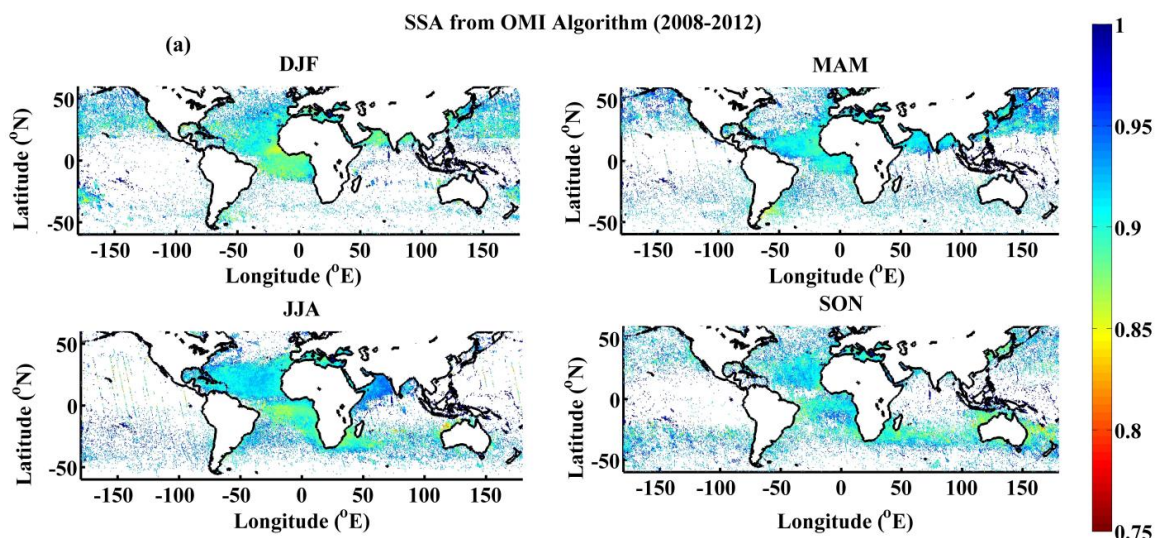
728

729

730

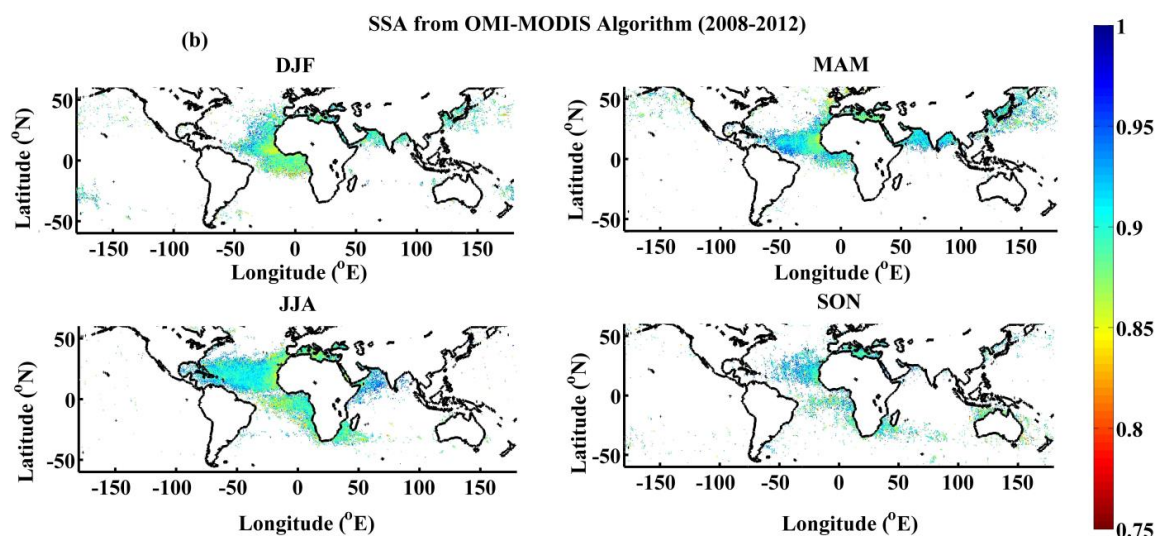
731

732



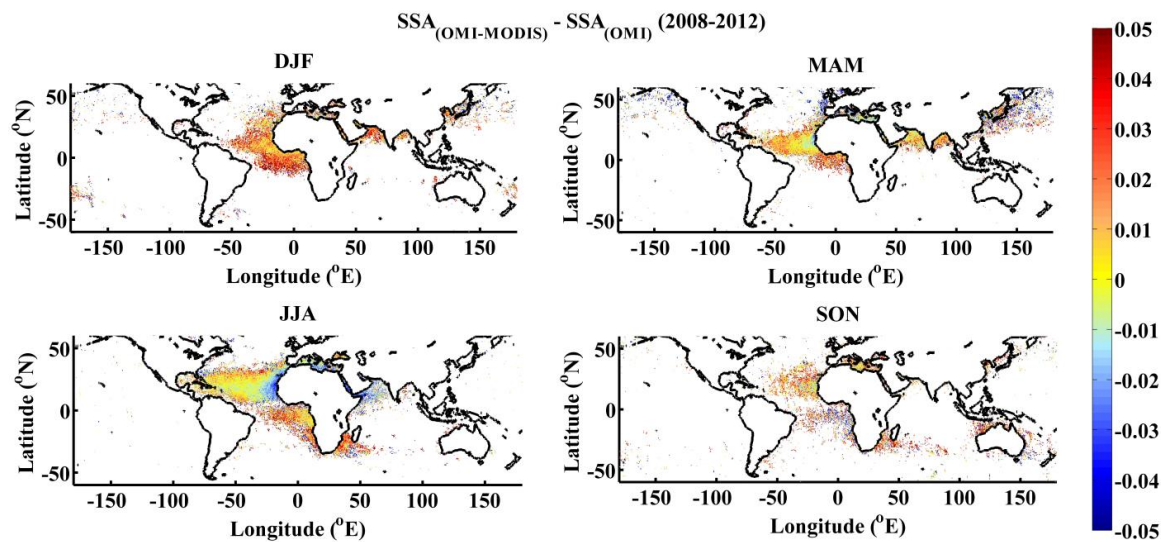
733

734 **Figure 1a.** Spatial distribution of SSA retrieved by OMI



735

736 **Figure 1b.** Spatial distribution of SSA retrieved by OMI-MODIS



737

738 **Figure 2.** Spatial distribution of difference in SSA retrievals

739

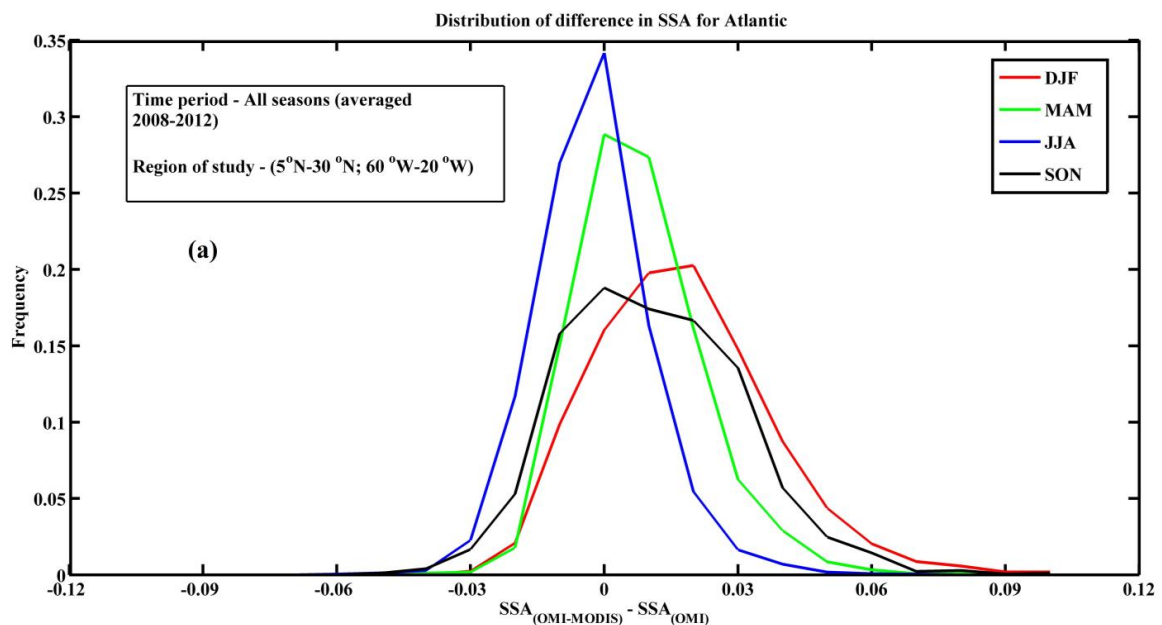
740

741

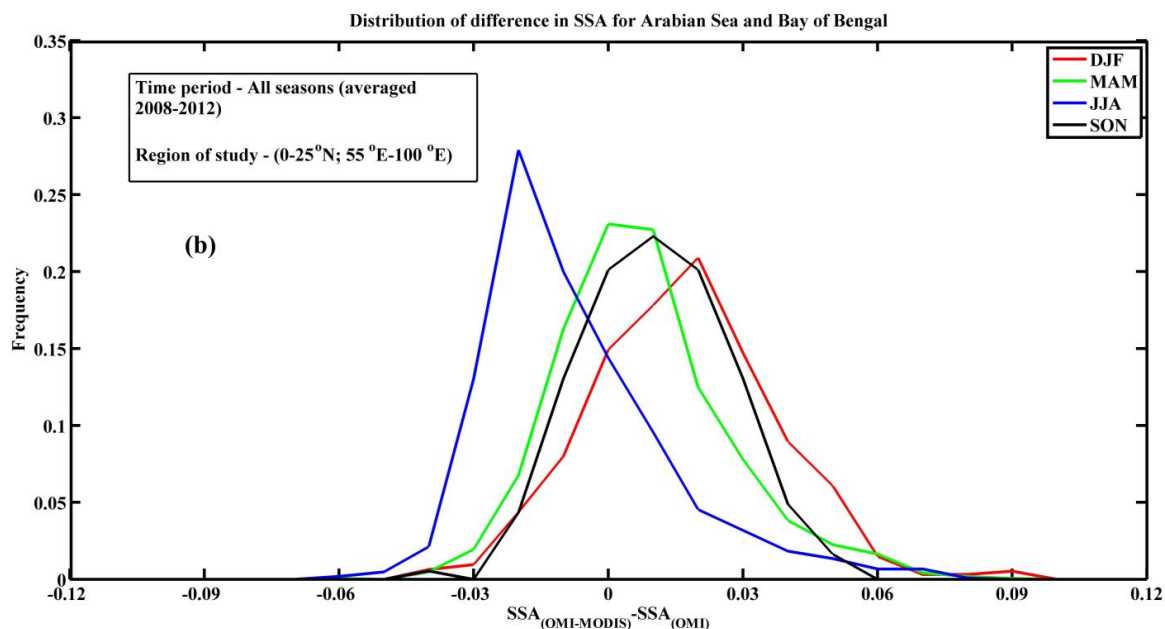
742

743

744



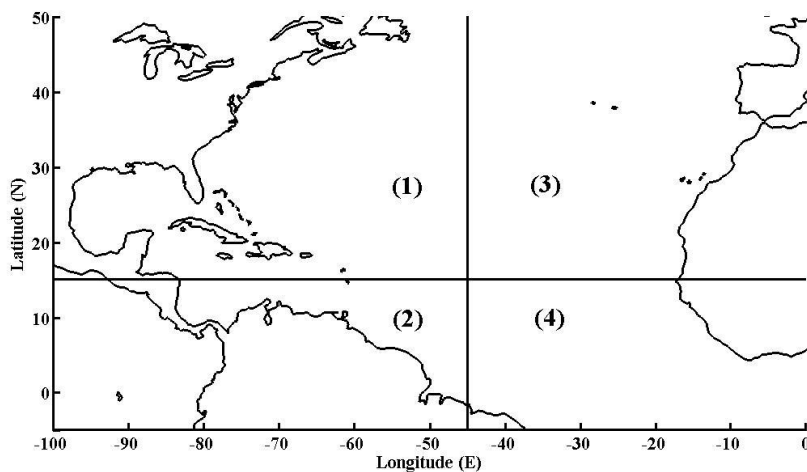
745



746

747 **Figure 3.** Distribution of difference in SSA for all seasons averaged over 2008-2012 over a)

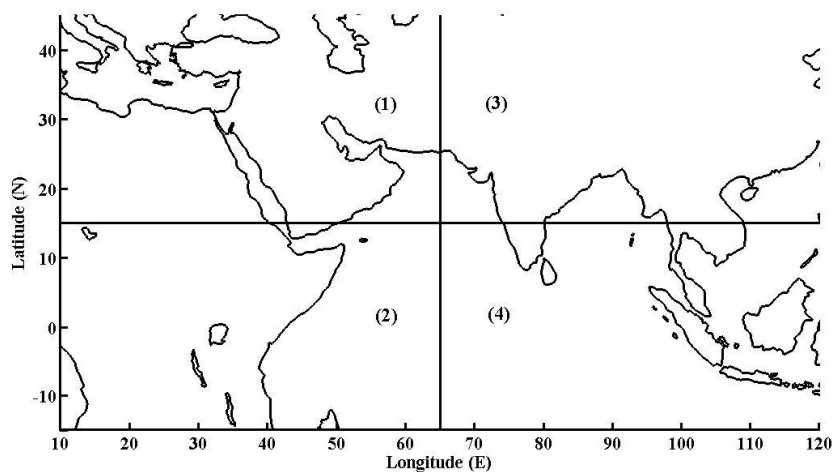
748 Atlantic and b) Arabian Sea and Bay of Bengal



749

750 **Figure 4.** Regions representing the various aerosol sources over Atlantic Ocean. 1) North

751 America, 2) Central/South America, 3) North Africa and 4) Southern Africa.

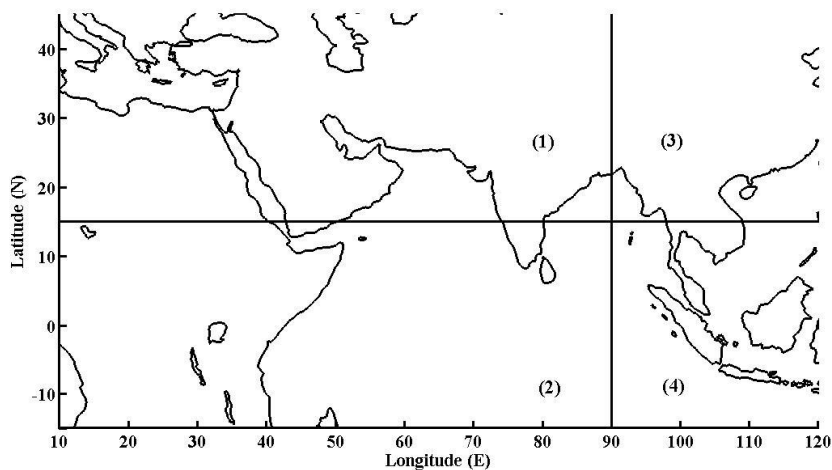


752

753 **Figure 5.** Regions representing the various aerosol sources over Arabian Sea. 1) Arabian

754 Peninsula and North Africa, 2) Southern Africa, 3) Indian sub-continent and 4) Indian Ocean and

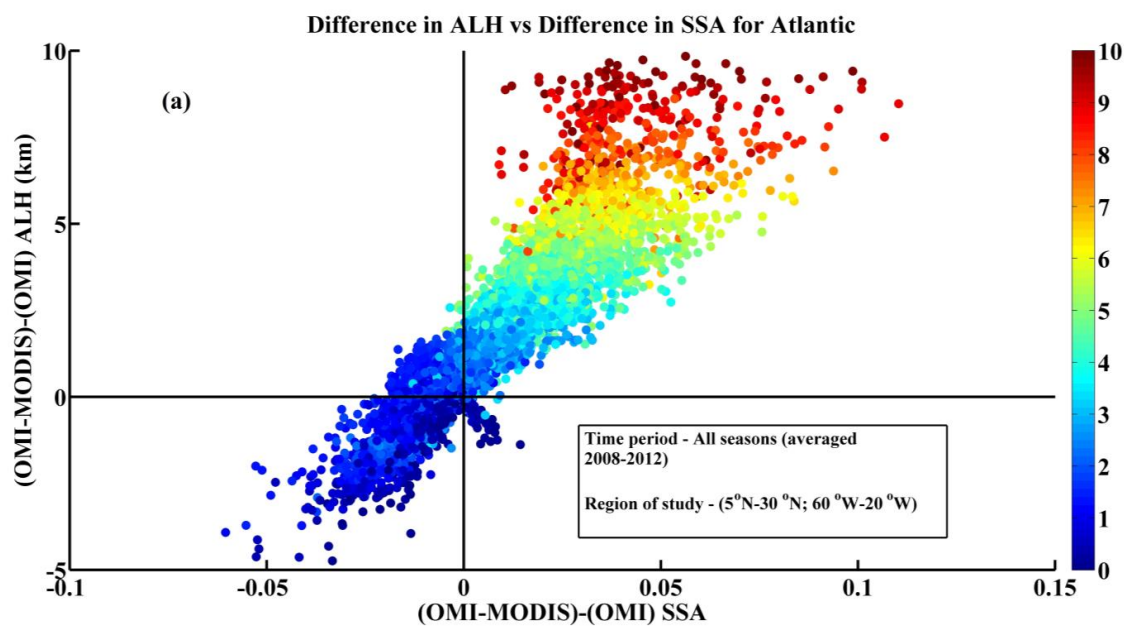
755 Southeast Asia.



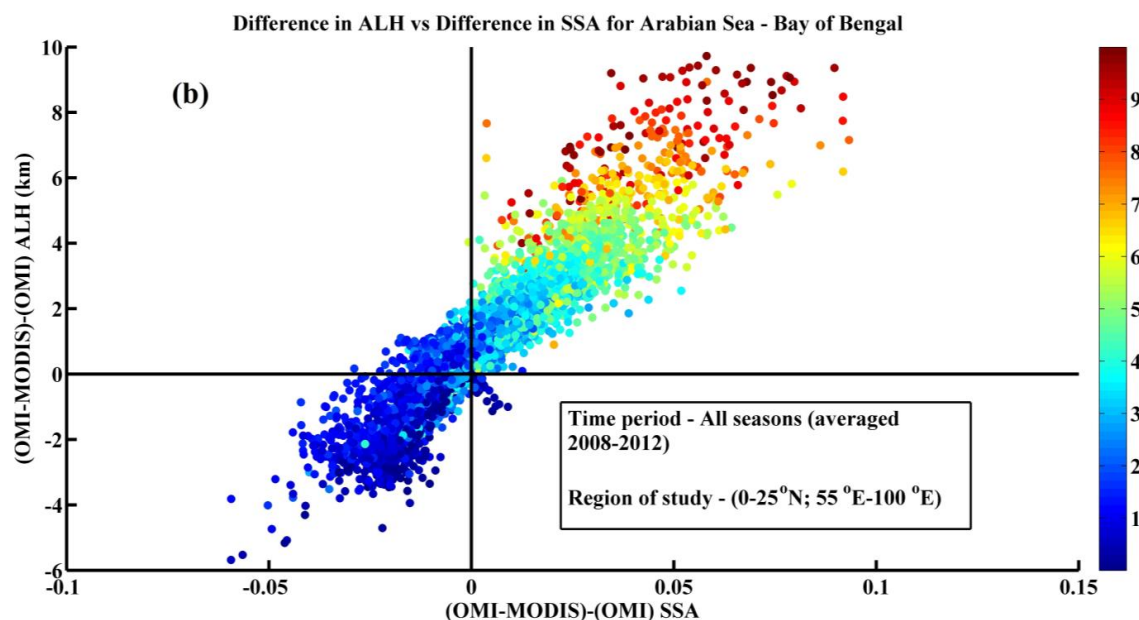
756

757 **Figure 6.** Regions representing the various aerosol sources over Bay of Bengal. 1) India/Arabian

758 Peninsula, 2) Indian Ocean, 3) North/Northeast India and East Asia and 4) Southeast Asia.

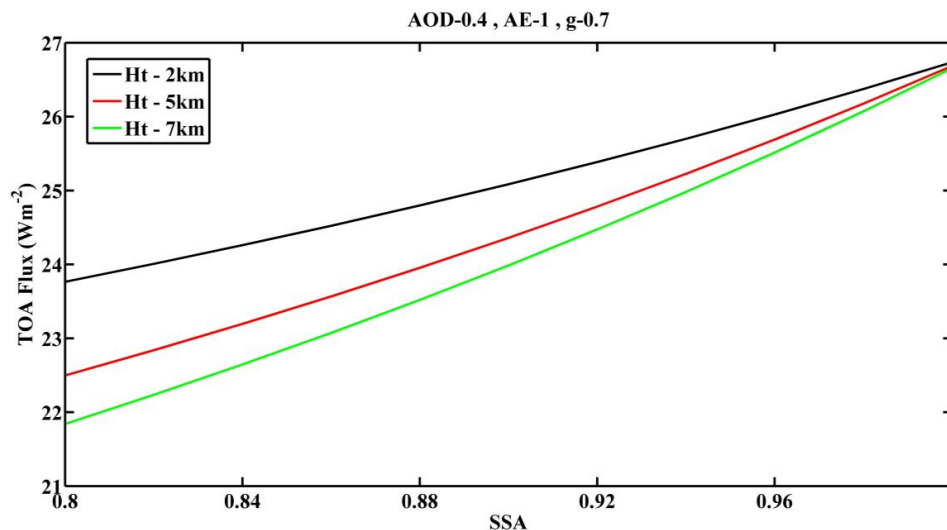


759



760

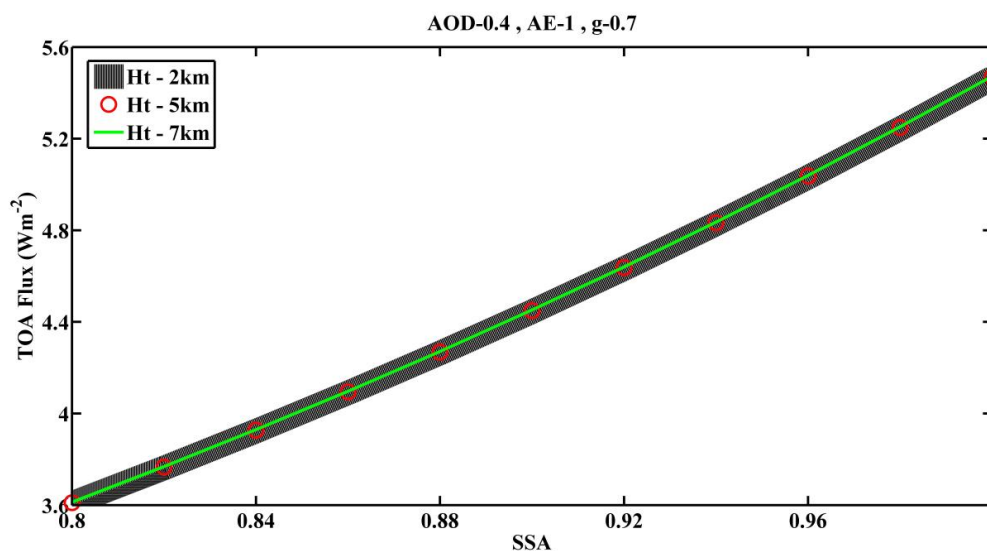
761 **Figure 7.** Difference in aerosol layer height (ALH) between OMI-MODIS and OMI vs.
 762 difference in SSA over a) Atlantic and b) Arabian Sea and Bay of Bengal. The colorbar
 763 represents ALH estimated by OMI-MODIS algorithm. At lower height (dark blue circles) OMI
 764 assumes ALH greater than that of OMI-MODIS and results in overestimation of SSA.



765

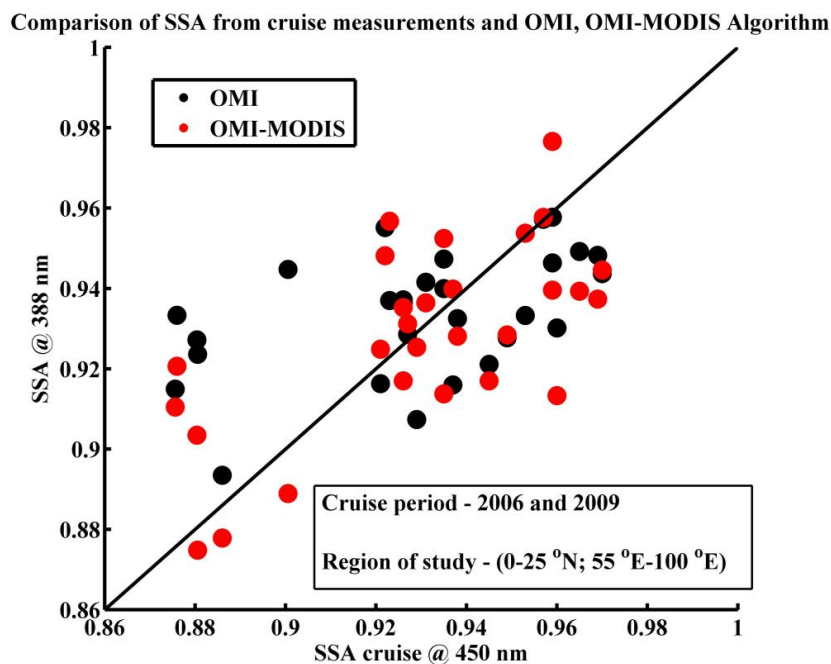


766 **Figure 8.** TOA flux calculated from SBDART for different SSA and ALH for UV (300-400nm)



767

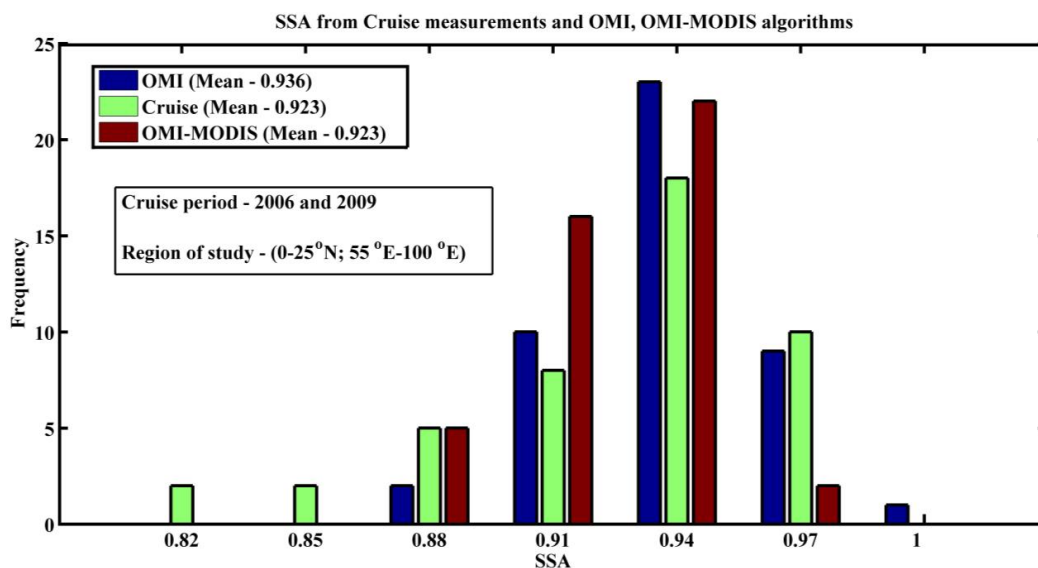
768 **Figure 9.** TOA flux calculated from SBDART for different SSA and ALH with Rayleigh
769 scattering removed for UV (300-400nm)



770

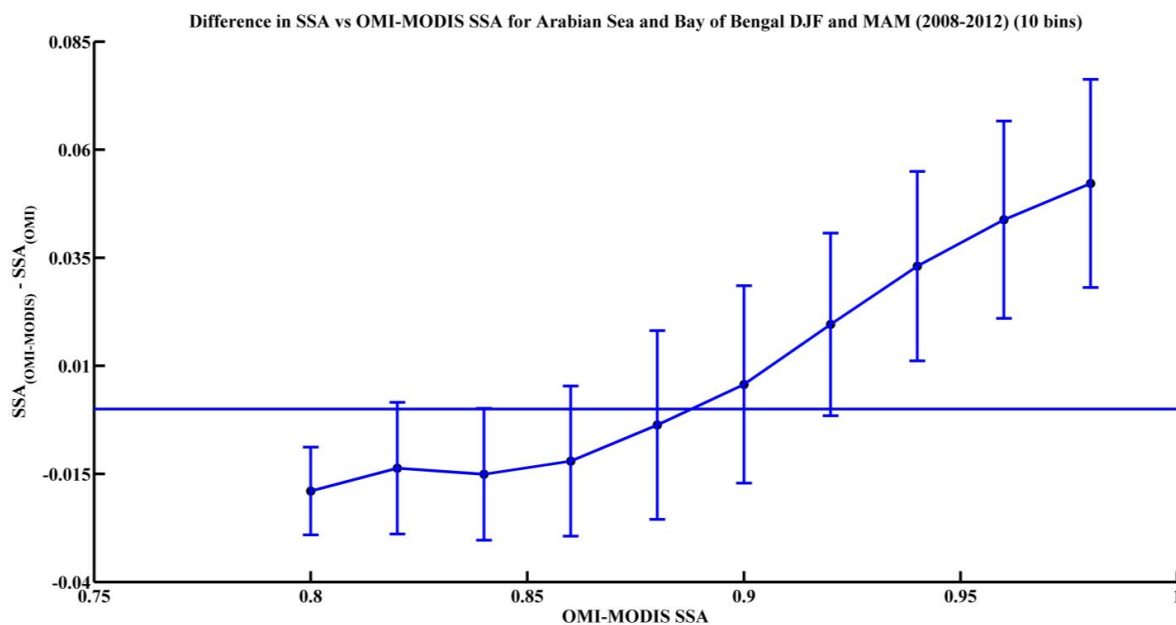


771 **Figure 10.** Comparison of SSA_{OMI}, SSA_{OMI-MODIS} with cruise measurements spatially averaged



772

773 **Figure 11.** Distribution of SSA from OMI-MODIS, OMI and cruise measurements.



774

775 **Figure 12.** Difference in SSA from OMI-MODIS and OMI Vs SSA from OMI-MODIS. OMI



776 overestimates SSA when absorbing aerosols are detected by OMI-MODIS.

777

778

779

780

781

References	Method	Technique	Limitation
Herman et al., 1975; King, 1979; Eck et al., 1998; Dubovik and King, 2000; Torres et al., 2005	Ground-based observations	Inverse methods measurements of solar radiances and/or aerosol properties along with radiative transfer calculations	Measurements are spatially and temporally constrained
Dubovik et al., 2002	Global network – Aerosols Robotic Network (AERONET)	Inverse technique using near-real time measured direct and diffuse radiation	Only land-based, low coverage over remote oceanic regions



Kaufman, 1987;	Critical surface	Over varying surface	Limited spatial
Zhu et al., 2011;	reflectance - where the	reflectance, the	variability of surface
Wells et al., 2012	net role of aerosol	radiance difference	reflectance. Works
	absorption and	between clear and hazy	only for few cases
	scattering becomes	skies is measured using	where there are large
	independent of aerosol	satellite images	amount absorbing
	optical thickness and is		aerosols present
	affected only by SSA		
Kaufman et al., 2002b	Retrieve SSA in visible wavelengths	Sun-glint is used as a bright background to differentiate role of scattering from aerosol absorption	Only limited scenarios present and does not work on land when absorbing aerosols are present (Torres et al., 2005).
Diner et al., 1998; Remer et al., 2005	Multi Angle Imaging Spectroradiometer (MISR) and Moderate Resolution Imaging Spectroradiometer (MODIS)	Retrieves AOD and SSA in the visible and infrared region of solar spectrum	Surface reflectance influences the retrievals



Herman et al., 1997; Torres et al., 1998	Total Ozone Mapping Spectrometer (TOMS)	Aerosol index parameter is highly sensitive to the Rayleigh scattering thus acting as a bright background in the UV regime	Large pixel size prone to cloud contamination
Torres et al., 2002	Ozone Monitoring Instrument (OMI)	Similar technique as TOMS. Pre-defined aerosol models used.	Sensitive to aerosol layer height and still prone to cloud contamination

782

783 **Table 1.** Ground-based and Satellite-based indirect methods to retrieve SSA

784

Seasons	Regions	1		2		3		4	
		2009	2010	2009	2010	2009	2010	2009	2010
DJF	500m	38%	40%	0%	0%	57%	45%	5%	15%
	1500m	43%	45%	0%	0%	24%	20%	33%	35%
	2500m	52%	50%	10%	10%	5%	15%	33%	25%
MAM	500m	9%	19%	0%	0%	86%	62%	5%	19%
	1500m	33%	38%	0%	4%	53%	29%	14%	29%
	2500m	38%	24%	19%	0%	29%	33%	14%	43%



JJA	500m	5%	5%	0%	0%	90%	90%	5%	5%
	1500m	9%	5%	0%	0%	67%	76%	24%	19%
	2500m	0%	5%	0%	0%	76%	76%	24%	19%
SON	500m	5%	5%	0%	0%	86%	71%	9%	24%
	1500m	0%	10%	0%	0%	81%	71%	19%	19%
	2500m	10%	14%	0%	0%	71%	57%	19%	29%

785

786 **Table 2.** Influence of various aerosol sources over Atlantic Ocean given as percentage of
 787 trajectories originating from each source respectively. The maximum influence is given in black
 788 bold. The different source regions are explained in text and Fig. 4.

789

Seasons \ Regions		Regions			
		1	2	3	4
DJF	500m	57%	0%	38%	5%
	1500m	62%	10%	19%	9%
	2500m	81%	14%	0%	5%
MAM	500m	19%	43%	19%	19%
	1500m	29%	29%	23%	19%
	2500m	57%	14%	24%	5%
JJA	500m	0%	24%	0%	76%
	1500m	19%	67%	0%	14%
	2500m	62%	33%	5%	0%



SON	500m	5%	24%	47%	24%
	1500m	14%	19%	48%	19%
	2500m	38%	10%	19%	33%

790

791 **Table 3.** Influence of various aerosol sources over Arabian Sea given as percentage of
 792 trajectories originating from each source respectively. The maximum influence is given in black
 793 bold. The different source regions are explained in text and Fig. 5.

794

Seasons \ Regions		1	2	3	4
		DJF	500m	72%	0%
	1500m	48%	14%	10%	28%
	2500m	29%	33%	0%	38%
MAM	500m	19%	48%	0%	33%
	1500m	57%	29%	20%	14%
	2500m	71%	24%	0%	5%
JJA	500m	0%	100%	0%	0%
	1500m	5%	95%	0%	0%
	2500m	14%	81%	0%	5%
SON	500m	5%	52%	33%	10%
	1500m	5%	43%	43%	9%
	2500m	5%	33%	29%	33%



795

796 **Table 4.** Influence of various aerosol sources over Bay of Bengal given as percentage of
797 trajectories originating from each source respectively. The maximum influence is given in black
798 bold. The different source regions are explained in text and Fig. 6.

799

	OMI	OMI-MODIS
Mean SSA (Cruise – 0.923)	0.936	0.923
Std. Dev. (Cruise – 0.04)	0.021	0.021
p- value	0.046	0.981
Confidence Interval	[0.0002, 0.027]	[-0.013,0.013]

800

801 **Table 5.** Comparison of SSA between both the satellite algorithms and cruise measurements

802